Preliminary PIV measurement of an air jet

Cite as: AIP Conference Proceedings **2047**, 020001 (2018); https://doi.org/10.1063/1.5081634
Published Online: 28 November 2018

Daniel Duda

Preliminary PIV Measurement of an Air Jet

Daniel Duda[1, a)]

[1]Faculty of Mechanical Engineering, University of West Bohemia in Pilsen

[a)]Corresponding author: dudad@kke.zcu.cz

Abstract. The planar Particle Image Velocimetry (PIV) technique has been used to study a jet flow of air. The nozzle diameter is 5 cm and output velocity ranged from 8 to 160 m/s corresponding to diameter based Reynolds number $2.6 \cdot 10^4$ – $5.5 \cdot 10^5$. The spatial resolution is 0.9 mm per Interrogation Area (IA) in all cases, which does not allow us to distinguish small vortices, but the development at scale comparable to the nozzle diameter can be studied.

INTRODUCTION

The experimental visualization method *Particle Image Velocimetry* (PIV) is used to study the jet flow [1] near the nozzle exit. The jet generator is developed for calibration of direction sensitive pressure probes; at this moment, it is in a preparation stage without final nozzle. The provisional nozzle has been printed by using a 3D-printer and it is shown in photography in Figure 1. This preliminary nozzle has output diameter 50 mm, the slow part has diameter 200 mm and contains only a single grid, which is not sufficient for production of a *potential core* with no turbulence inside. Additionally, the 3D-printing technology produces a surface roughness, as is apparent in Figure 1, which shortens the transition to turbulence in the boundary of the jet core [1]. The aims of this work are to test the ability of measuring fast air flows by using PIV technique and to prepare data for comparing the "cheap" nozzle with the carefully developed one, which will be tested in the future.

Measurement of output velocity of the air

First, there is roughly measured the mean velocity of the jet core in dependence on the relative settings of the control unit of the jet compressor. Dynamical pressure is measured by using the differential barometer between the Pitot tube localized approximately in the axis of the jet oriented against the flow, thus measuring the *total pressure*, and the ambient pressure, which is thought to be equal to the *static pressure*. Then the velocity is obtained from equation:

$$p_d = \frac{1}{2}\rho u^2, \tag{1}$$

where u is the unknown flow velocity, p_d is the dynamic pressure, and ρ is the density of the fluid, in this case it is considered to be $\rho = 1.15$ kg/m^3. The comparison of pressure velocimetry and particle image velocimetry is plotted in Figure 2.

At the maximum rotor frequency, 130 Hz, the flow reaches the velocity 164 m/s. The maximum flow velocity of the final jet generator with a better nozzle is expected to be smaller, around ~ 150 m/s, due to additional honeycombs and grids planned to suppress the turbulence in the low-velocity part.

SPATIAL DISTRIBUTION OF THE VELOCITY

The experimental measurement method of *Particle Image Velocimetry* (PIV) [2] is based on suspending small particles into the studied flow and observing the motion of these particles illuminated by a laser defocused in one direction in order to illuminate a plane. The particles are droplets of glycerin solution produced by commercially

17th Conference of Power System Engineering, Thermodynamics and Fluid Mechanics
AIP Conf. Proc. 2047, 020001-1–020001-7; https://doi.org/10.1063/1.5081634
Published by AIP Publishing. 978-0-7354-1773-1/$30.00

available Safex fog generator. During the data analysis, we *expect* that the particle follows the motion of the fluid and we measure the mean displacement between two *interrogation areas* (IA) separated by a time- and space-interval. These *interrogation areas* are a basic cell of the resulting Figure of spatial velocity distribution obtained by using the PIV method.

In the here published measurement, the size of one interrogation area has been chosen to be 0.92 mm, which is quite large value for a such fast flow [2], but this value allows us to map the entire width of the jet flow close to the nozzle exit. In the future, we plan to measure smaller areas with better resolution. The relative localization of the studied area and the jet nozzle is shown in Figure 3 (a).

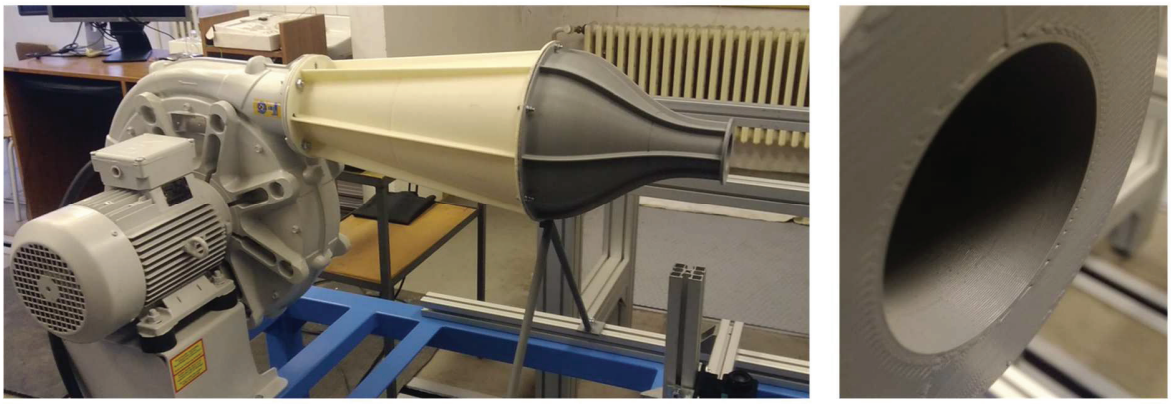

FIGURE 1. The photograph of the jet generator with the preliminary nozzle. Note the surface roughness typical for the 3D-printing technology.

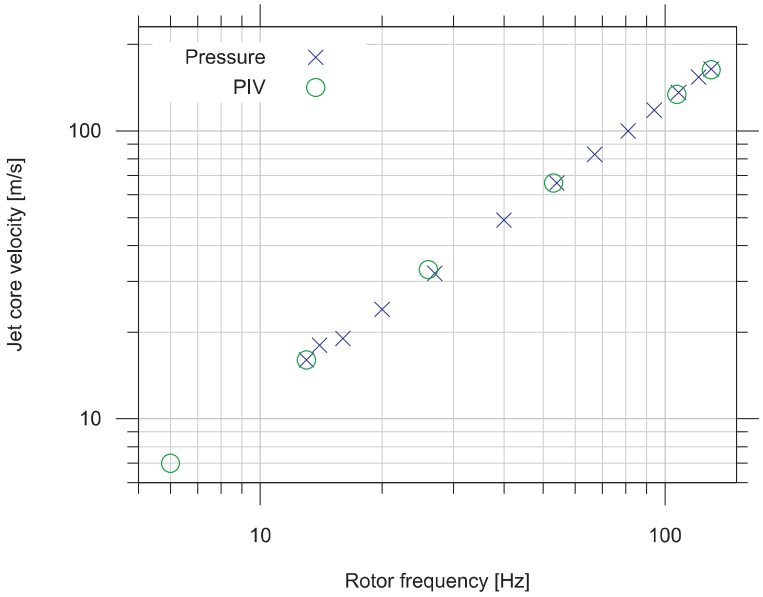

FIGURE 2. The dependence of jet core velocity on the frequency of the jet generator rotor measured by two approaches: Blue crosses denotes the pressure difference measurement while the green circles correspond to the average velocity of the particles carried in the 2.5 cm subarea at the center of the jet.

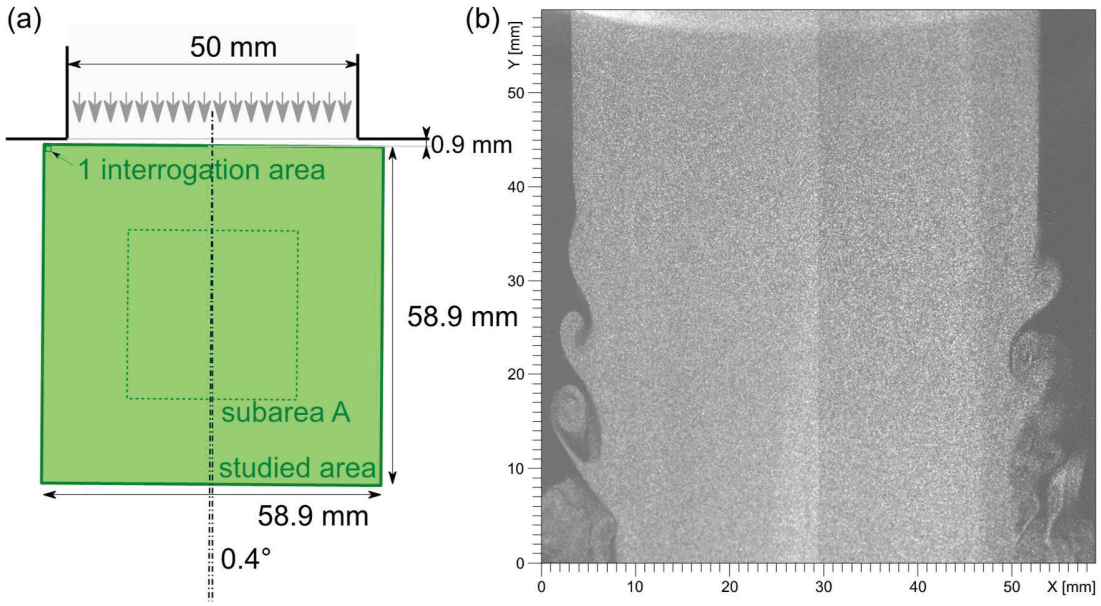

FIGURE 3. Left (a): the sketch of the relative localization of the studied area and the jet nozzle. Right (b): a typical instantaneous photograph of the particles illuminated by the laser sheet, the actual flow velocity is 7.9 m/s corresponding to nozzle diameter based Reynolds number Re = $2.6 \cdot 10^4$.

The time interval between two consecutive frames ΔT should correspond to the velocity of the studied flow in such a way, that the displacement of the particle is sufficient, but not too far, because then the analysis algorithm is unable to find the correct correlation. The used analysis algorithm is called *Adaptive PIV* of the Dantec Dynamic studio and it guarantees subpixel accuracy, which, in addition to the large interrogation area displacement, theoretically leads to dynamical resolution of velocity in order of 10^2 (the ratio of the largest and smallest measurable velocity), but the trustworthy values are closer to the dynamical resolution of 10^1. This is one of the weakness of the PIV method among other velocimetries: the small dynamical resolution in a single measurement. ΔT in this measurement varied between 4 – 100 μs, see table 1 for more details.

Lets note, that in the right-hand-side of the Figure 3 there are no particles outside of the jet stream, therefore the velocity cannot be measured there. If we want to study the flow in such areas (for example the suction), we had to add particles there, but then those left in the jet core. It is quite difficult to obtain data from a single realization of flows containing mixing of fluids of different velocities. In all following Figures, there is displayed velocity of only that fluid, which passed the nozzle.

TABLE 1: Individual measurements at different frequencies f_{rotor} of the compressor rotor. ΔT is the chosen time interval between consecutive frames. $u|_A$ is the mean velocity in the subarea A (see Figure 3), this column is plotted in Figure 2. E, E_{TFD} and E_{mean} are the total kinetic energy of the flowfield, the kinetic energy of the *temporal fluctuation decomposition* (TFD) and the kinetic energy of the *mean* over 100 statistically independent samples. The values are calculated without using any additional parameter, which would increase the uncertainty; this causes the unit [mJm^2/kg] – if one wants to know the energy in [mJ], he has to multiply this value by the fluid density (approximately 1,15 kg/m^3) and the thickness of the illuminated plane (ca 1 mm). I_T is the turbulence intensity and "$|_A$" in the last three columns indicates that the corresponding quantity is calculated in the subarea A.

f_{rotor}	ΔT	Re	$u\|_A$	E	E_{TFD}	E_{mean}	I_T	$E\|_A$	$E_{TFD}\|_A$	$I_T\|_A$
[Hz]	[μs]		[m/s]	[mJm^2/kg]	[mJm^2/kg]	[mJm^2/kg]	[%]	[mJm^2/kg]	[mJm^2/kg]	[%]
6,5	100	$2{,}6 \cdot 10^4$	7,87	$8{,}9 \cdot 10^1$	1,2	$8{,}8 \cdot 10^1$	11,5	$2{,}7 \cdot 10^1$	$4{,}5 \cdot 10^{-2}$	4,10
13,13	50	$5{,}4 \cdot 10^4$	16,2	$3{,}8 \cdot 10^2$	8,6	$3{,}7 \cdot 10^2$	15,1	$1{,}1 \cdot 10^2$	$5{,}1 \cdot 10^{-1}$	6,68
26,65	25	$1{,}1 \cdot 10^5$	33	$1{,}6 \cdot 10^3$	$3{,}1 \cdot 10^1$	$1{,}6 \cdot 10^3$	14,1	$4{,}7 \cdot 10^2$	3,2	8,20
53,3	12	$2{,}2 \cdot 10^5$	66,3	$6{,}5 \cdot 10^3$	$1{,}4 \cdot 10^2$	$6{,}4 \cdot 10^3$	14,7	$1{,}9 \cdot 10^3$	$1{,}3 \cdot 10^1$	8,26
107,3	6	$4{,}5 \cdot 10^5$	134	$2{,}6 \cdot 10^4$	$5{,}3 \cdot 10^2$	$2{,}6 \cdot 10^4$	14,4	$7{,}8 \cdot 10^3$	$4{,}1 \cdot 10^1$	7,27
130	4	$5{,}5 \cdot 10^5$	163	$3{,}8 \cdot 10^4$	$5{,}1 \cdot 10^2$	$3{,}8 \cdot 10^4$	11,6	$1{,}2 \cdot 10^4$	$4{,}3 \cdot 10^1$	6,11

Temporal fluctuation decompositions

Instantaneous realizations are considered *statistically independent* due to the used camera framerate[1] f_{cam} = 5 Hz. They all look similarly as the averaged velocity field plotted in Figure 4, therefore they are not reprinted here. The average velocity field displays the homogenous jet core, which narrows due to the growing instability at the interface of the jet fluid and the surroundings, which is visualized in Figure 4 by the sum of velocity variances.

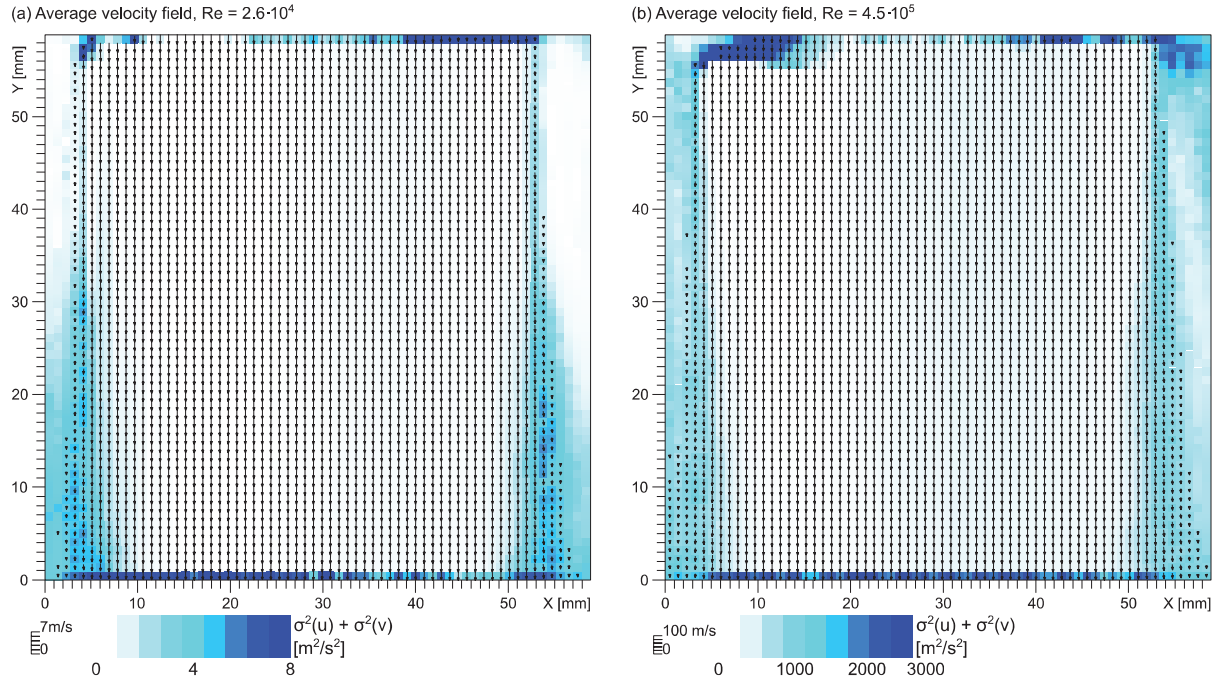

FIGURE 4 The average velocity fields for two jet velocities: Re = $2.6 \cdot 10^4$ (a) and Re = $4.5 \cdot 10^5$. The length scale is 919 μm/IA, The color of individual IAs corresponds to the sum of variances of x and y velocity component, for values see the legend under each panel. The large amplitudes of variances at top and bottom boundary are not relevant, because in this region the particles leave the field of view; therefore the searching of maximum correlation fails there often.

The flow structures can be highlighted by using the, so-called, Reynolds fluctuation decomposition, which is a difference of each instantaneous realization and the time average shown in Figure 4:

$$\vec{u}_{\mathrm{TFD}}(\vec{x},t) = \vec{u}(\vec{x},t) - \langle \vec{u} \rangle_t(\vec{x}), \tag{2}$$

where the subscript TFD denotes the *temporal fluctuation decomposition*. An example snapshot of temporal fluctuation decomposition for 2 different velocities is shown in Figure 5. In order to decrease the noise, the vector field is convoluted with a Gaussian function with half-width of 1 IA = 0.9 mm. This operation dumps all structures under 1 IA, which contain the noise *and* the real physical information as well.

Reynolds fluctuation decomposition can be performed not only "classically" in the time direction; it is possible to decompose the flow-field into average and fluctuation component also in respect to *space* [3]. This approach offers more maneuvering possibilities in the data with better spatial resolution than temporal (which is the case of PIV). While, in the time direction, we have only one interval between consecutive pairs of frames ($\Delta t_{cam} = 1/f_{cam}$ = 200 ms), which is so long, that it is not possible to follow the development of the flow structures in time, in the spatial domain, on the other hand, we can work with intervals starting from 1 IA (0.9 mm) up to the size of the camera field of view, which is, in this case, 64 IA = 58.9 mm. One can protest, that the Kolmogorov scale η, whose magnitude can be estimated by using the characteristic length (nozzle aperture diameter, L = 50 mm), kinematic viscosity $\nu = 1.5 \cdot 10^{-5}$ m^2/s and a characteristic velocity u = 8 – 160 m/s as

$$\eta \sim \left(\frac{\nu^3 L}{u^3}\right)^{\frac{1}{4}} \sim 10\ \mu\mathrm{m} \tag{3}$$

[1] This is the frequency between the *pairs of frames*, the frames in the pair are separated by the above mentioned time interval ΔT in order of microseconds.

is much smaller than the size of 1 IA in all of here discussed cases. However, at least the upper part of the *inertial subrange* can be visualized focusing to variety of structure sizes in the range from few IA up to the size of the field of view [4]. Theoretically, the smallest studied scale can be 1 IA, but this scale is strongly affected by the noise.

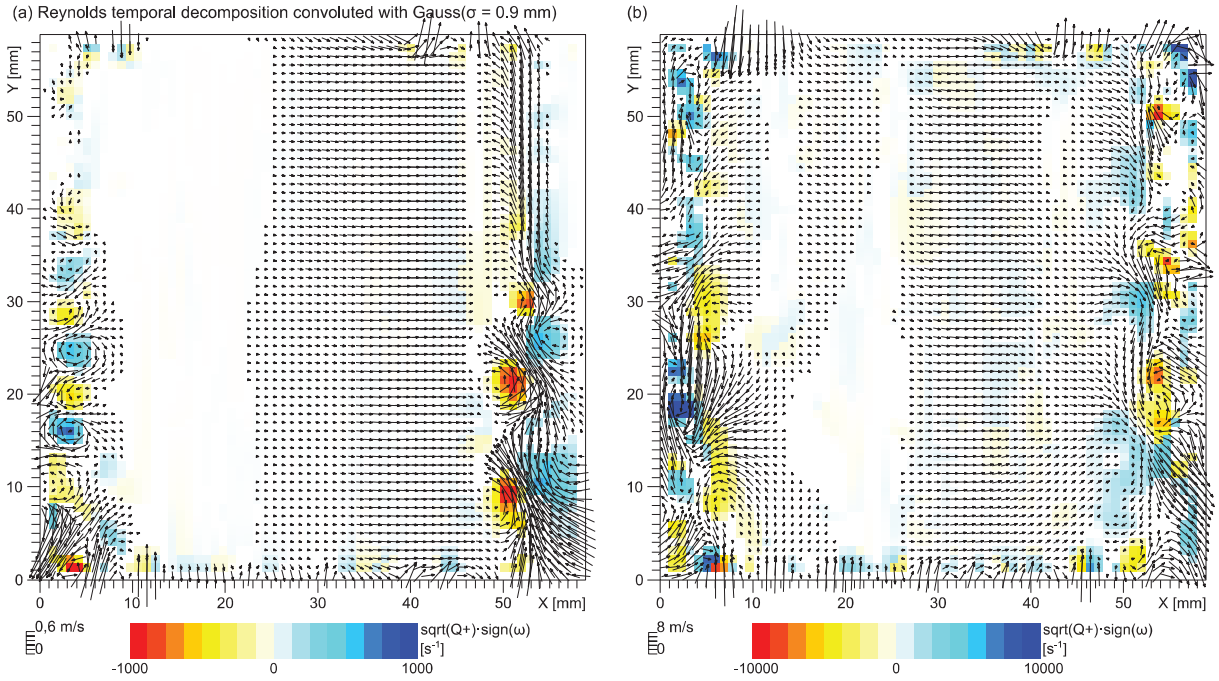

FIGURE 5: An example of the time-decomposed velocity field for two velocities: Re = $2.6 \cdot 10^4$ (a) and Re = $4.5 \cdot 10^5$ (b). The color corresponds to square root of positive part of the Q invariant of the velocity gradient tensor multiplied by the sign of vorticity.

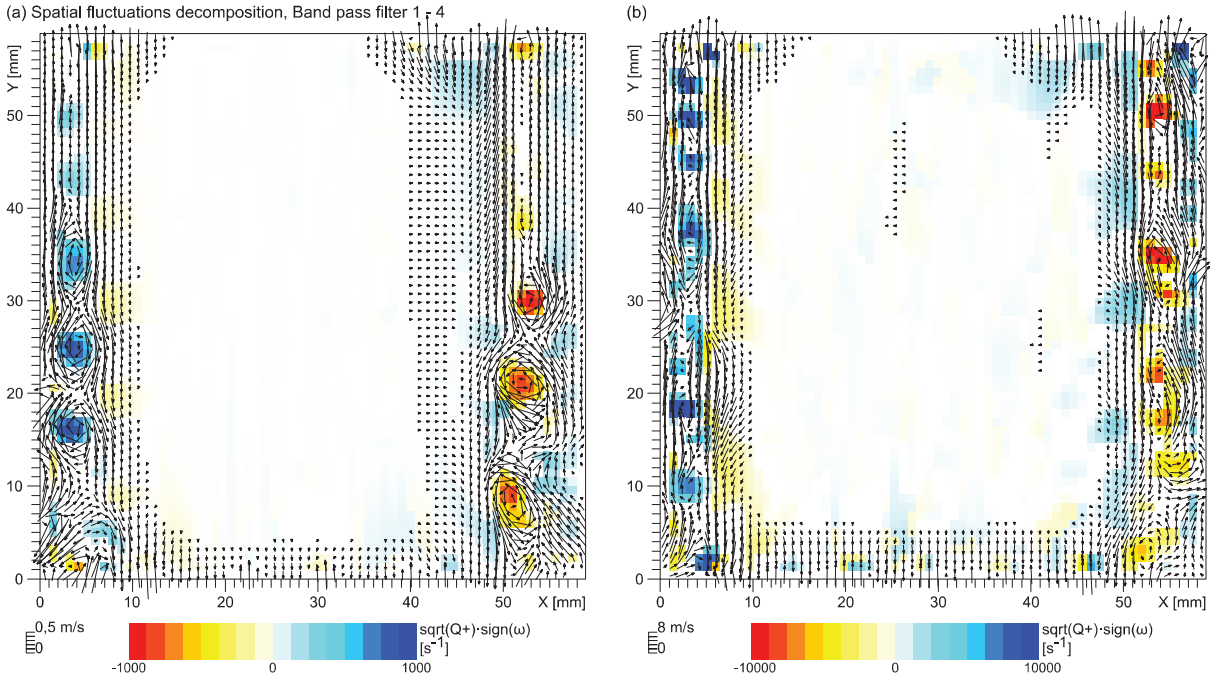

FIGURE 6: An example of spatial fluctuation decomposition for two jet velocities: Re = $2.6 \cdot 10^4$ (a) and Re = $4.5 \cdot 10^5$ (b). The color corresponds to square root of positive part of the Q invariant of the velocity gradient tensor multiplied by the sign of vorticity.

Figure 6 shows measured velocity field with highlighting the scales from 2 to 8 mm calculated by using a convolution with *band pass filter* with halfwidths σ_1 = 1 mm and σ_2 = 4 mm,

$$\vec{u}_P = \vec{u}(\vec{x}, t) * [G(\vec{x}; \sigma_1) - G(\vec{x}; \sigma_2)], \tag{4}$$

where G denotes the Gaussian function with halfwidth σ

$$G(\vec{x}; \sigma) = \frac{1}{\sqrt{2\pi}\sigma} e^{-\frac{x^2}{2\sigma^2}}. \tag{5}$$

The color-map of both Figures 5 and 6 shows the local value of the square root of the positive part of Q invariant of the velocity gradient tensor multiplied by the vorticity sign;

$$\sqrt{Q^+}\frac{\omega}{|\omega|}, \tag{6}$$

where

$$Q = \frac{1}{2}(\omega^2 - s^2) = \frac{1}{2}(tr^2(\nabla\vec{u}) - tr(\nabla\vec{u})^2). \tag{7}$$

Its unit therefore is the same as the unit of vorticity, i.e.s^{-1}, and, additionally, the color shade distinguishes orientation of the fluid rotation similarly, as the vorticity would do.

Both Figures 5 and 6 shows the *Kelvin-Helmholtz* instability in the shear layer between the surroundings and the potential jet core. Its development is evident even from the Figure 3. Let's note, that there are no information from the surroundings, although both Reynolds decomposition methods show a non-zero vectors there. While in the case of spatial decomposition, which works only with one instantaneous velocity field snapshot, this issue corresponds to the expectation of zero velocity in the surroundings, in the case of temporal decomposition is this issue a product of the non-stationarity of the jet; roughly speaking: in some frames we have information from those areas, in some not, but the average, which is subtracted from *all* frames, is calculated only with using signal from *some* frames. This can be nicely shown by comparing the left-hand sides of Figure 5(a) and 6(a), which both shows exactly the same snapshot. In the case of temporal decomposition (Figure 5(a)), it is evident, that the whole jet was little bit shifted to the left in respect to the average position, therefore the velocity corresponding to the core is subtracted from the undulating shear layer, which leads to the appearance of a wake of alternating vortices. The same area analyzed via spatial approach shows a wake of one-direction vortices, which better corresponds to the physics of the Kelvin-Helmholtz instability.

Discussion

Table 1 shows, among others, the energetic balance of the center of the jet core denoted as subarea A in the Figure 3(a). Similar quantity measured for the entire field of view has no physical meaning due to the cylindrical symmetry and due to the gradually developing Kelvin-Helmholtz instability. By measuring the kinetic energy of the temporal fluctuation decomposed (TFD) velocity field we can calculate the intensity of turbulence I_T

$$I_T = \frac{\sqrt{\langle(\vec{u} - \langle\vec{u}\rangle_t)^2\rangle_t}}{\langle|\vec{u}|\rangle_t} = \sqrt{\frac{E_{\mathrm{TFD}}}{E_{\mathrm{mean}}}}, \tag{8}$$

where

$$E = \frac{1}{2}\int \rho u^2 \mathrm{d}A, \tag{9}$$

In all cases, the turbulence intensity is smaller than 10 %, but we have to keep in mind the restriction in the dynamic range of PIV in velocity as well as the fact, that the fluctuation component itself is already averaged over one interrogation area, therefore the turbulence at scales smaller than 1 IA is unobservable by using the PIV technique at this resolution. However, the energy content of the turbulence at length-scales smaller than 1 IA increases with Reynolds number due to the elongation of the inertial subrange of the cascade. This statement can explain the counter-intuitive observation that the measured turbulence intensity *decreases* at larger velocities – it does not decrease, it just becomes invisible.

Figure 7(a) shows the energy content of the jet core as a function of characteristic wave number of contributing structures. Note, that the *slope* of the energy content is similar for all velocities at largest scales (smaller wave number), but, at small scale, the smaller velocities already display dumping, while the larger ones decrease not so fast. From the measured data, we are not able to calculate the total fluctuation energy content, because we do not see the end of the cascade.

Figure 7(b) shows the relative change of this energy content highlighting the sudden increment at the smallest structures, which is believed to be caused by the instrument noise produced e.g. by incorrect localization of peak of maximum correlation or other rough errors during the data analysis procedure. The fact, that this effect is visible only in plot of change, suggests that the instrument noise is small. Note that the relative change of the smallest velocity (blue pentagon in Figure 7) crosses one at length-scale 1.7 mm suggesting the maximum energy content at this scale.

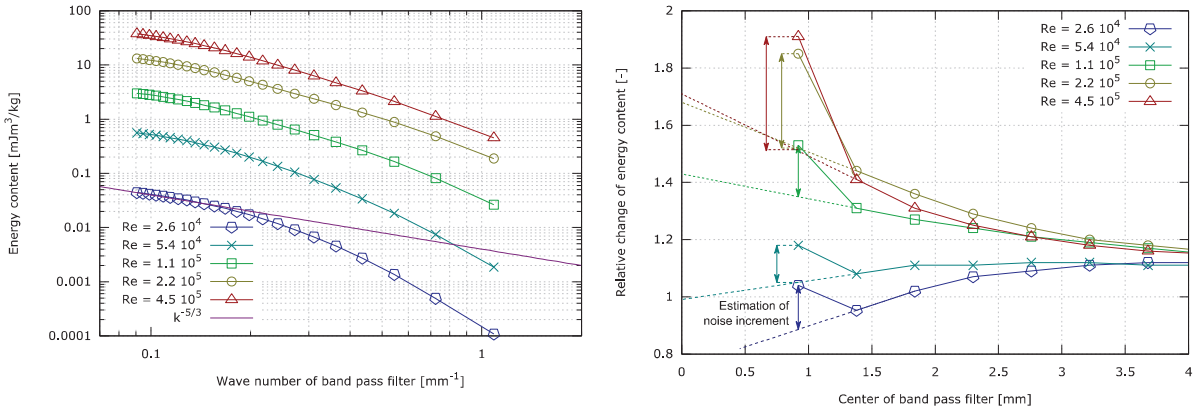

FIGURE 7: Left (a) energy content of spatial fluctuations as a function of the width of the band pass filter in the central region of the jet core (subarea A in Figure 3). The *width* of the band pass filter is 1 IA in all points. Right (b) relative change of energy content plotted in (a); dashed lines represent the estimation of trend in contrast to the steep increase of the first point, which is incremented by the instrument noise.

CONCLUSIONS

We have experimentally studied the airflow in the initial part of a jet, focusing on the central jet-cross-section of length slightly larger than the nozzle exit diameter. The main motivation was to verify, if the current PIV (Particle Image Velocimetry) instrumentation is able to measure velocities up to 160 m/s and, at the same time, it is able to distinguish turbulent structures in the studied fluid. We found that the PIV velocity measurement agrees with the pressure measurement, which is a standard tool for this kind of flows. Additionally, we have shown that PIV is able to detect big vortices produced by the Kelvin-Helmholtz instability at the jet core boundary and that spatial decomposition to fluctuation component offers a physically more trustworthy picture than the temporal decomposition (this is not a general rule – it depends on the case). Estimation of the instrument noise, which we believe to act only at length-scale of *one* interrogation area suggest, that this noise is relatively small compared with the turbulence, which is believed to act at all scales. The used resolution is inadequate for studying the flow down to the dissipation subrange, and we will have to use smaller *interrogation area* in future experiments.

ACKNOWLEDGMENTS

This work has been supported by the project SGS-2016-045 (Increase of efficiency, reliability and a lifespan of power machines and devices 4). Author thanks to prof. Václav Uruba for valuable discussions, to ing. Jan Uher for help with pressure probe and to ing. Bohumil Laštovka for technical support with the experiment realization.

REFERENCES

1. E. J. List, Annual Review of Fluid Mechanics 14, 189-212 (1982)
2. V. Kopecký, *Metody laserové anemometrie v experimentální mechanice tekutin* (Technická univerzita v Liberci, Liberec, 2001).
3. A. Agrawal and A. Prasad, Experiments in Fluids 33(4), 565-577 (2002).
4. A. Agrawal, Experiments in Fluids 39, 836 (2005).